Fibers and Polymers 2012, Vol.13, No.4, 507-514 DOI 10.1007/s12221-012-0507-z

Preparation and Properties of Polypropylene Nanocomposites Reinforced with Exfoliated Graphene

Ji-Eun An, Gil Woo Jeon, and Young Gyu Jeong*

Department of Materials Design Engineering, Kumoh National Institute of Technology, Gumi 730-701, Korea
(Received September 8, 2011; Revised November 18, 2011; Accepted November 20, 2011)

Abstract: We have prepared a series of polypropylene/exfoliated graphene (PP/EG) nanocomposite films via efficient melt-compounding and compression, and investigated their morphology, structures, thermal transition behavior, thermal stability, electrical and mechanical properties as a function of EG content. For the purpose, EG, which is composed of disordered graphene platelets as reinforcing nanoscale fillers, is prepared by the oxidation/exfoliation process of natural graphite flakes. SEM images and X-ray diffraction data confirm that the graphene platelets of EG are well dispersed in PP matrix for the nanocomposites with EG contents less than 1.0 wt%. It is found that thermo-oxidative degradation of PP/EG nanocomposites is noticeably retarded with the increasing of EG content. Electrical resistivity of the nanocomposite films was dramatically changed from ~10^{16} to ~10^{6} Ω·cm by forming electrical percolation threshold at an certain EG content between 1 and 3 wt%. Tensile drawing experiments demonstrate that yielding strength and initial modulus of PP/EG nanocomposite films are highly improved with the increment of EG content.

Keywords: Exfoliated graphene, Polypropylene, Electrical property, Mechanical property, Thermal stability

Introduction

Polypropylene (PP) is one of chief polyolefins in commercial importance because of its cost-effectiveness as well as intrinsic properties of low density, high stiffness, good tensile strength, and inertness toward acids, alkalis and solvents [1]. PP has been thus used in a wide range of applications including packaging, textiles (ropes, thermal underwear and carpets), automotive components, and so on. On the other hand, for advanced applications, physico-chemical properties of PP need to be further improved or new functionalities should be endowed.

In the simplest case, adding appropriate nanoscale fillers to a polymer matrix can enhance its performances, often in very dramatic degree, by maximizing the nature and properties of the fillers [2,3]. This strategy is particularly effective in yielding high performance nanocomposites, when good dispersion of the nanoscale fillers with high aspect ratio and/or high surface area to volume ratio is achieved and properties of the fillers are substantially better than those of the polymer matrix, for example, reinforcing a polymer matrix by much stiffer and/or multi-functional nanofillers such as ceramics [4-6], clays [7-9], and carbon nanotubes [10-13].

Recently, graphene platelets are considered as an intriguing and interesting new class of reinforcing nanoscale carbon material with many unusual and fascinating properties of thermal stability, mechanical modulus, and electrical and thermal conductivity [14-16]. Accordingly, there are several reports on preparation and property characterization of PP-based nanocomposites including expanded graphite or commercially available graphite nanoplatelets, i.e., xGnP^{TM}, as the reinforcing nanofiller [17-22]. Shen *et al*. reported structure and electrical properties of grafted PP/graphite nanocomposite prepared by solution intercalation [17]. In the study, the conducting percolation threshold of the nanocomposites was found to be 0.67 vol%, which was much lower than that of the conventional composites prepared by melt mixing. Causin *et al*. reported that PP/conductive graphite composites, which were prepared by melt-mixing, exhibited an enhanced thermal conductivity as well as different crystallization mechanism due to the presence of graphite nanofiller [18]. On the other hand, Drazal *et al*. have fabricated PP nanocomposites reinforced with xGnP by using various methods of melt-mixing, polymer solution and coating, and compared their mechanical and electrical properties [19]. The coating method was found to be more effective than the solution method, in terms of lowering the electrical percolation threshold. In addition, Drazal's group has also systematically studied the thermal expansion coefficient, thermal conductivity, rheological property, and oxygen gas permeability of PP/xGnP nanocomposites [20]. Recent research of Torkelson's group reported that PP/graphite nanocomposites prepared via solid-state shear pulverization exhibited effective dispersion and mechanical property enhancement [22]. On the other hand, it should be mentioned that graphite or xGnP used for manufacturing PP/graphite nanocomposites in literatures had well layered structure of graphene platelets, although it was a nanoscale filler [19]. In addition, highly layered structure of graphites or xGnP remained in the nanocomposites.

Recently, it has been reported by Aksay's group that exfoliated graphene (EG), which is composed of at least 80 % single graphene sheets and has the average thickness of ~1.75 nm, can be manufactured in bulk quantities through rapid thermal expansion of graphite oxide (GO), which was

*Corresponding author: ygjeong@kumoh.ac.kr

obtained by oxidization of natural graphite (NG) flake via Staudenmaier's method [23,24]. Therefore, it is considered that EG prepared via the oxidation/exfoliation process can be also used as the effective nanoscale reinforcing filler for PP. In this study, we have prepared EG nanofiller, which is composed of disordered graphene platelets, and fabricated a series of PP/EG nanocomposites with a variety of EG contents *via* simple but efficient melt-mixing. Effects of graphene platelets on thermo-oxidative stability, crystallization/melting behavior, electrical resistivity, and tensile mechanical performance of the neat PP are systematically investigated.

Experimental

Materials

Isotactic polypropylene (melt flow rate of 1.0 g/10 min at 230 °C and 2.16 kg by ASTM D-1238, maleic anhydride of 0.8 wt%) was kindly supplied by WooSung Chemical Co., Ltd., Korea. Natural graphite (NG) flake (grade 3061) with a mean diameter of ~500 μm was purchased by Sigma-Aldrich Com. Sulfuric acid (90 %) and nitric acid (60 %) was purchased from Junsei Chemical Co., Ltd. Potassium chlorate (99.5 %) was purchased from Kanto Chemical Co., Ltd. All the chemicals were used without further purification.

Preparation

As the reinforcing filler, exfoliated graphene (EG) were manufactured via the oxidation/exfoliation process suggested by Akasy's group [23-25]. Firstly, graphite oxide (GO) was obtained by the oxidation of NG flakes. Sulfuric acid (360 m*l*) and nitric acid (180 m*l*) were stirred in an 1 *l* round-bottom flask, which was cooled in an ice bath for 30 min. NG flake (20 g) was added into the mixed acid solution with vigorous stirring for 20 min. Potassium chlorate (220 g) was slowly added over 15 min into the reaction flask, which was located in an ice bath. Oxidation of NG flake was carried out for 120 hrs. After the reaction, GO slurry in the solution was washed with distilled water and filtrated, which was repeated until neutral pH was attained. GO filtrate was dried at room temperature for 24 hrs. Finally, EG was obtained by thermal expansion of GO at 1050 °C for 30 sec and it was used for reinforcing nanofiller for PP matrix.

For manufacturing PP/EG nanocomposites vial melt-compounding, PP chips were mechanically ground into powders, which were mixed with the predetermined amount of EG in a mechanical mixer. The EG content in solid mixtures was set to be 0.0, 0.1, 0.3, 0.5, 0.7, 1.0, 3.0, 5.0, 7.0 and 10.0 wt%. Each solid mixture was then melt-compounded by using a modular intermeshing co-rotating twin screw extruder (BK-11, Bowtec Com., Korea) with screw length of 40 mm and screw diameter of 11 mm. Melt-compounding temperature from zone 1 to Zone 6 was controlled to be 170, 175, 180, 190, 200 and 200 °C, and the screw seed of 180 rpm was applied. The melt-compounded PP/EG strand was cut into pellets, which were then dried under vacuum at 70 °C for 24 hrs. Melt-quenched neat PP and its nanocomposite films with 0.2 mm thickness were prepared by hot-pressing the composite pellets at 190 °C for 3 min and quickly quenching into an iced water bath at 0 °C. Finally, each nanocomposite films were vacuum-dried at 25 °C over 24 hrs before structure and property characterization.

Characterization

The structural order and crystalline feature of NG, GO, EG, and PP/EG nanocomposite films were characterized by using a Rigaku X-ray diffractometer with Ni-filtered Cu-Kα radiation (40 kV and 150 mA) at a scanning rate of 2 °/min.

The dispersion state of EG in the nanocomposites were examined by a scanning electron microscope (JEOL JSM-6380LV). For comparison, SEM images of NG, GO, and EG were also obtained.

Thermal transition behavior of the neat PP and its nanocomposite films with various EG contents was characterized by using a differential scanning calorimeter (Diamond DSC, Perkin Elmer Inc.). DSC heating and cooling thermograms under nitrogen gas environment were obtained in the temperature range of 0~200 °C at a heating and cooling rate of 10 °C/min.

Thermo-oxidative stability of the neat PP and PP/EG nanocomposite films was examined by using a thermogravimetric analyzer (TGA Q500, TA Instrument). TGA experiments were performed under oxygen gas condition from room temperature to 600 °C at a heating rate of 20 °C /min.

Electrical volume resistivity of the neat PP and PP/EG nanocomposite films measured by using a electrometer/high resistance meter (6517A, Keithley Instruments) with 8009 resistivity test fixture.

Tensile mechanical properties of the nanocomposite films were investigated by using a universal testing machine (UTM, Instron series 4467) at 25 °C. Film sample sizes for the tensile drawing experiment were $5.0\times40.0\times0.2$ mm^3. The sample gauge length was 20.0 mm and the cross-head speed was 20.0 mm/min.

Results and Discussion

Structural Characterization

Figure 1 shows X-ray diffraction patterns as well as SEM images of NG, GO, and EG. In the X-ray diffraction pattern of NG, a strong diffraction peak was detected at 26.4 °, which corresponds to a *d*-spacing of 0.336 nm according to Bragg's law expressed as $n\lambda=2d\sin\theta$, where n is an integer determined by the given order and λ is the X-ray wavelength. The presence of strong diffraction peak confirms that the pristine NG flake has a highly ordered packing structure of

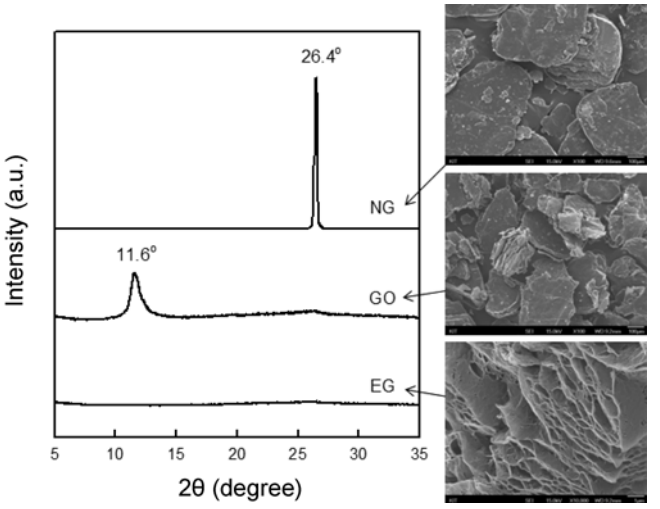

Figure 1. X-ray diffraction patterns and associated SEM images of natural graphite (NG), graphite oxide (GO), and exfoliated graphene (EG).

graphene platelets. In case of GO, a relatively weak and broad diffraction peak was observed at 11.6 °, which is associated with *d*-spacing of 0.763 nm. The diffraction peak appeared at 11.6 ° is related to the increment of the interlayer distance between graphene platelets owing to functional groups introduced into NG flakes during the oxidation process. On the other hand, EG do not show any diffraction peak, which means that graphene platelets were totally exfoliated and disordered during the rapid thermal expansion process. This disordered and exfoliated structure of EG was also confirmed by SEM image, as shown in Figure 1.

Figure 2 displays X-ray diffraction patterns of neat PP and its nanocomposite films with various EG contents. In case of the neat PP film, sharp diffraction peaks of typical α-form crystal, which is the most stable among polymorphs, are appeared. For all nanocomposite films, X-ray diffraction patterns are almost identical to that of the neat PP film without showing any diffraction peaks from ordered graphene platelets. These results denote that only PP α-form crystals are developed dominantly in the nanocomposites and graphene platelets of EG in the PP matrix remain in disordered structure. In addition, it was found the presence of graphene platelets in the nanocomposites do not affect the crystalline α-phase of PP matrix.

To have a better comprehension of the dispersion state of graphene platelets of EG in the nanocomposites, SEM images of the neat PP and its nanocomposite films fractured cryogenically were obtained, as can be seen in Figure 3. For the nanocomposites with low EG contents up to 1.0 wt%, no aggregates of graphene platelets were detected in the PP matrix (Figure 3(b)~(d)). It means that graphene platelets of EG are uniformly distributed in the PP matrix. On the other hand, in cases of the nanocomposites with high EG contents

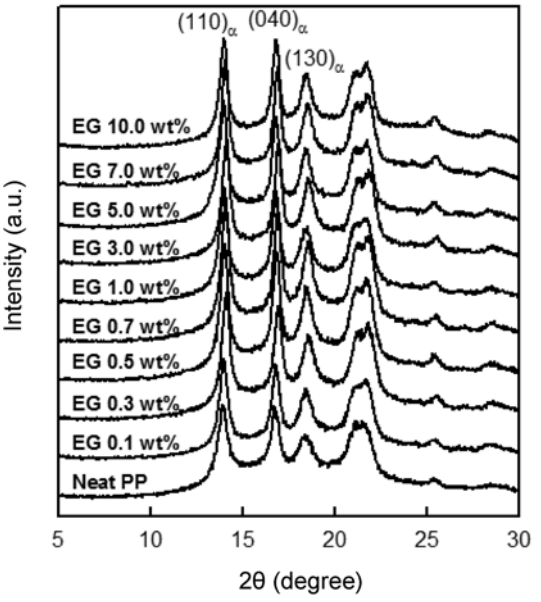

Figure 2. X-ray diffraction patterns of neat PP and PP/EG nanocomposites including various EG contents.

above 3.0 wt%, partial aggregates of graphene platelets were observed (Figure 3(e)~(f)), although they did not exhibit any ordered structural feature, which was confirmed by X-ray diffraction patterns in Figure 2. The presence of aggregated graphene platelets of EG is probably due to the partial restacking of disordered graphene platelets in the nanocomposites with high EG contents. It has been recently reported that, when the amount of graphene platelets reaches a critical content, the distance among graphene platelets is so small that they can be stack together easily due to van der Waals force among graphene platelets [26]. From these results, it is conjectured that the critical EG content is between 1 and 3 wt% EG. As will be discussed in later, agglomeration of graphene platelets of EG in the PP matrix will influence thermal, electrical, and mechanical performances of the nanocomposites.

Thermal Properties of PP/EG Nanocomposites

Figure 4 shows DSC heating and cooling thermograms of the neat PP and its nanocomposite films containing various EG contents. In the heating thermograms of the melt-quenched film samples (Figure 4(a)), the melting transition temperature (T_m) remained unchanged, while the melting endothermic peak area (ΔH_m) decreased slightly with the increment of the EG content. On the other hand, in the cooling thermograms (Figure 4(b)), it was observed that the crystallization temperature (T_c) was shifted to higher temperatures, as the EG content increased in the nanocomposites. It demonstrates that the graphene platelets of EG dispersed in the nanocomposites promote the overall melt-crystallization of PP by serving as nucleating agents. From the DSC heating and cooling thermograms, characteristic

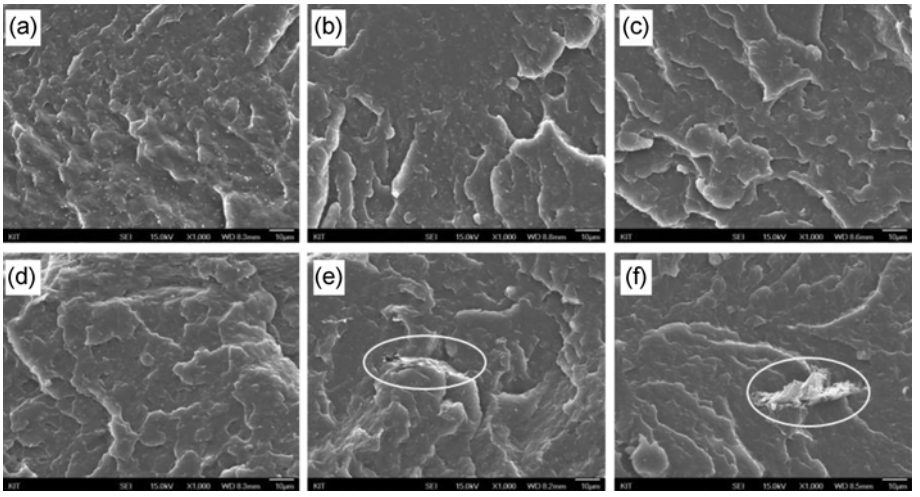

Figure 3. SEM images the cryogenically fractured surfaces for the neat PP and its nanocomposite films with various EG contents. (a) neat PP, (b) 0.3 wt% EG, (c) 0.7 wt% EG, (d) 1.0 wt% EG, (e) 3.0 wt% EG, and (f) 7.0 wt% EG.

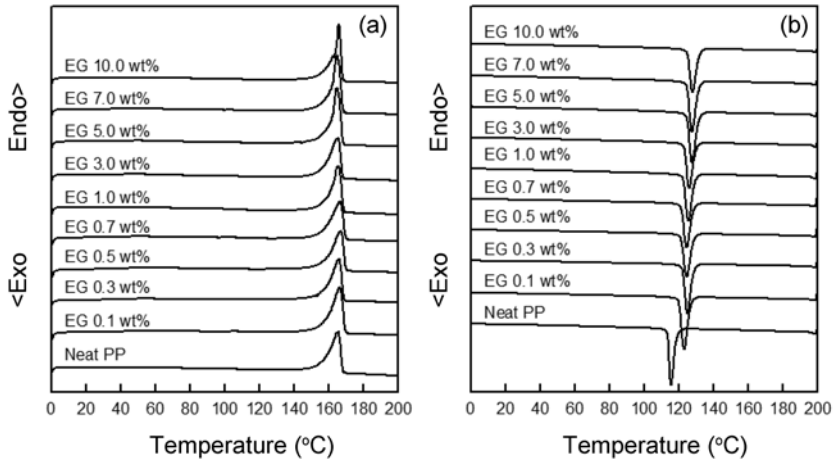

Figure 4. DSC heating (a) and following cooling (b) thermograms of the neat PP and its nanocomposite films with various EG contents.

melting/crystallization peak temperatures (T_m and T_c) and enthalpies (ΔH_m and ΔH_c) were evaluated and summarized in Table 1. To characterize the influence of graphene platelets of EG on the formation of PP crystals, the apparent crystallinity (X_c) of the samples could be calculated by using following equation:

$$X_c(\%) = \frac{\Delta H_m}{\Delta H_m^o \cdot \phi} \times 100 \quad (1)$$

where ΔH_m^o is the melting enthalpy (209 J/g) of the 100 % crystalline isotactic PP, ΔH_m^o is the melting enthalpy of the samples evaluated from the DSC heating thermograms, and ϕ is the weight fraction of PP in the nanocomposites. It was found that the apparent crystallinity of PP/EG nanocomposites was almost identical with that of the neat PP, regardless of EG content in the nanocomposite films within the experimental error (Table 1).

Enhanced thermal stability of PP is also very important for its applications. Accordingly, thermal stability of the neat PP and its nanocomposite films with various EG contents were examined under oxygen gas atmosphere, as can be seen in Figure 5(a). It was found that thermo-oxidative degradation of PP/EG nanocomposites under oxygen gas condition was noticeably retarded, compared with the neat PP. For quantitative comparison, thermo-oxidative degradation temperatures at 50 % weight loss ($T_{50\%}$) of the neat PP and its nanocomposites were evaluated and they were summarized in Table 1. $T_{50\%}$ value of the neat PP film was measured to be ~261 °C. In case of the nanocomposite film with 0.1 wt% EG, $T_{50\%}$ value was evaluated to be ~276 °C, which was ~15 °C higher than that of neat PP. For the nanocomposite film with 10 wt% EG, more highly improved thermo-oxidative degradation performance of $T_{50\%}$ ~301 °C was achieved. To examine thermo-oxidative degradation behavior in detail, the first derivative weigh loss curves for the neat PP and its nanocomposites were obtained, as shown in Figure 5(b),

Table 1. Thermal transition characteristics (T_m, ΔH_m, X_c, T_c, and ΔH_c) and thermal degradation temperature ($T_{50\%}$) for the neat PP and PP/EG nanocomposite films

Sample code	EG (wt%)	DSC heating runs			DSC cooling runs		TGA
		T_m (°C)	ΔH_m (J/g)	X_c (%)	T_c (°C)	ΔH_c (J/g)	$T_{50\%}$ (°C)
Neat PP	0.0	165.1	80.3	38.4	115.5	83.1	260.7
PP/EG	0.1	166.4	77.3	37.0	123.0	87.2	276.4
	0.3	165.7	76.6	36.8	124.9	87.0	268.5
	0.5	166.8	78.1	37.6	124.6	86.6	267.1
	0.7	166.4	75.6	36.4	124.6	85.8	281.8
	1.0	165.4	76.0	36.7	125.6	86.1	277.1
	3.0	165.2	73.0	36.0	126.1	83.1	290.0
	5.0	164.5	73.2	36.9	127.7	83.2	290.7
	7.0	164.6	71.6	37.4	127.7	81.0	304.5
	10.0	165.9	70.1	37.3	127.9	79.9	300.7

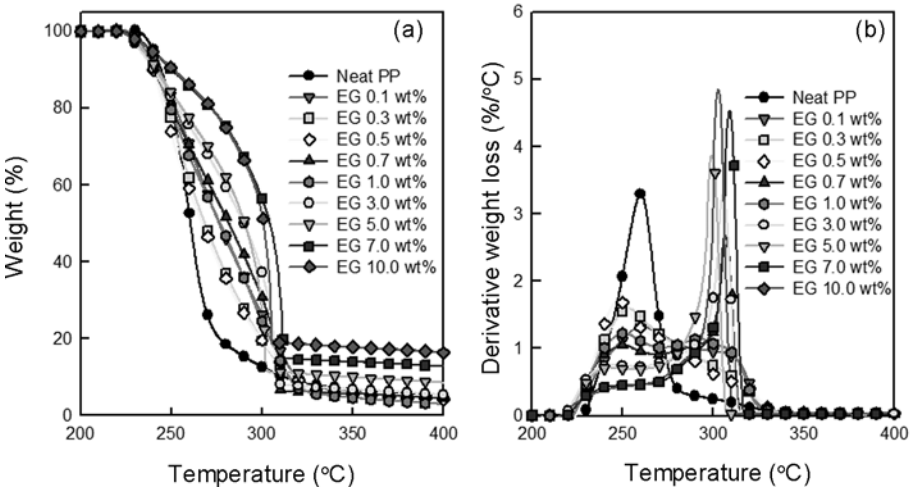

Figure 5. TGA thermograms (a) and their 1st derivative curves (b) of the neat PP and its nanocomposite films with various EG contents examined under oxygen gas condition.

where the thermo-oxidative degradation behavior of PP/EG nanocomposites was quite different from that of the neat PP. For instance, the neat PP film exhibited an intense weight loss peak at ~260 °C. In cases of PP/EG nanocomposites, two discernible weight loss peaks were observed, indicating a two-step mechanism of the thermo-oxidative degradation of the nanocomposites. The derivative weight loss peak intensity at lower temperature was decreased with increasing the EG content, whereas the peak intensity at higher temperature was substantially increased. It is thus expected that the weak weight loss peak at lower temperature of ~260 °C is due to the degradation of PP chains which are not influenced by the presence of graphene platelets of EG, while the strong weight loss peak at higher temperature of ~300 °C is related with the degradation of PP chains hindered by graphene platelets of EG. It was reported that PP/xGnP nanocomposites had high oxygen gas barrier performance even at low xGnP loading [19]. Considering that apparent crystallinity of PP/EG nanocomposite films is almost identical irrespective of the EG content, it is valid to contend that the highly improved thermo-oxidative stability of PP/EG nanocomposites under the oxygen gas condition is dominantly originated from the barrier effect of graphene platelets of EG dispersed in the PP matrix to the permeating oxygen gas molecules. It is also noticeable that no discernible difference in thermo-oxidative degradation behavior for the nanocomposite films with high EG contents above 3.0 wt% is associated with the existence of partial aggregates of disordered graphene platelets as can be seen in SEM images (Figure 3).

Electrical Properties of PP/EG Nanocomposites

Figure 6 shows the change of the electrical volume resistivity of PP/EG nanocomposite films as a function of the EG content. In case of the neat PP film, the electrical resistivity was measured to be ~10^{16} Ω·cm, which indicates

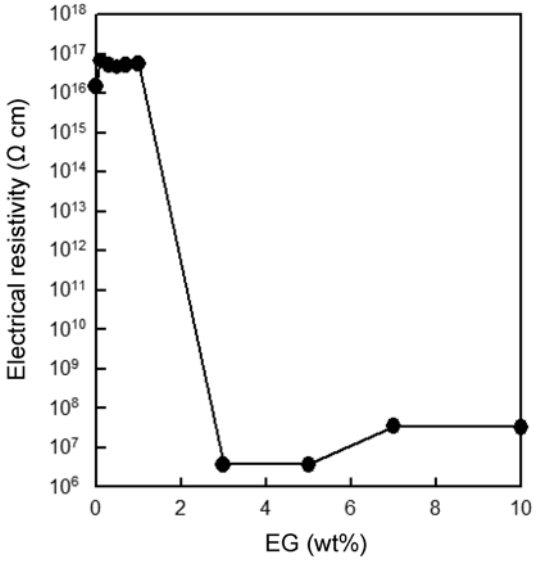

Figure 6. Electrical volume resistivities of the neat PP and its nanocomposite films as a function of EG content.

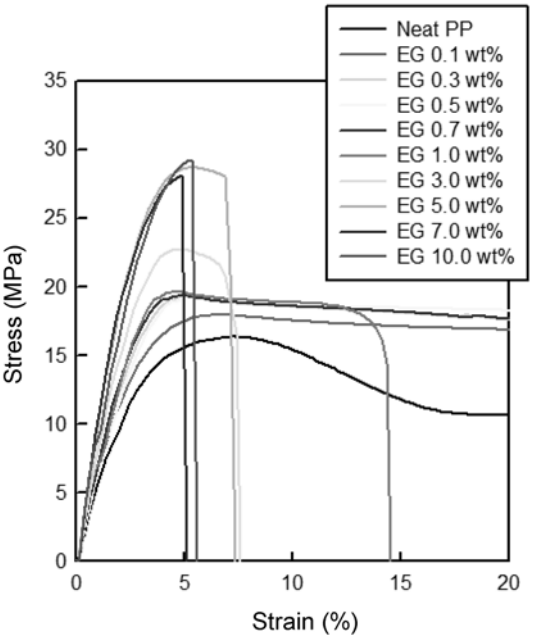

Figure 7. Stress-strain curves of the neat PP and its nanocomposite films at 25 °C.

that the neat PP film is electrically insulating. For the nanocomposite films with EG contents less than 1.0 wt%, the electrical resistivity of ~10^{16} Ω·cm was retained. On the other hand, in cases of the nanocomposites with high EG contents above 3.0 wt%, remarkably low electrical resistivity of 10^6~10^7 Ω·cm was attained. This electrical resistivity transition from insulating to semi-conductive materials can be explained by the percolation/hopping mechanism. It is reasonable to note that the electrical percolation threshold of PP/EG nanocomposite films by melt-compounding technique in this study was achieved at a certain EG content between 1.0 and 3.0 wt%. This result can be supported by the fact that nanocomposites with EG contents above 3.0 wt% exhibited aggregates of disordered graphene platelets owing to the van der Waals interaction among neighboring graphene platelets in the PP matrix. It is also noticeable that the electrical resistivity of 10^6~10^7 Ω·cm for PP/EG nanocomposites is low enough to be used for electrostatic dissipation applications.

Mechanical Properties of PP/EG Nanocomposites

In order to investigate the effect of graphene platelets of EG on mechanical properties of PP, uniaxial tensile tests for PP/EG nanocomposite films were carried out and the resulting stress-strain curves were presented in Figure 7. It was found that breaking strength and initial modulus of PP/EG nanocomposite films were highly increased by the introduction of graphene platelets, while breaking strain were decreased, as summarized in Table 2. On the other hand, the breaking strength for the neat PP film was somewhat higher than those of the nanocomposites with EG contents of 0.1~3.0 wt%, which is owing to the strength-hardening effect for the neat PP film during the tensile elongation after yielding. The overall mechanical data suggest that the tensile mechanical performance of the neat PP film is varied dramatically by the introduction of graphene platelets. For deep understanding the mechanical performances of PP/EG nanocomposite films, the initial modulus was plotted as a function of EG content, as can be seen in Figure 8, and they were compared with the values predicted by the Halpin-Tsai model. By assuming the random orientation of graphene platelets in the PP matrix, the theoretical composite modulus, $E_{composite}$, based on the Halpin-Tsai equation is expressed as [27-29]

$$E_{composite} = \left[\frac{3}{8} \frac{1+\frac{2}{3}\left(\frac{d_{EG}}{t_{EG}}\right)\eta_L V_{EG}}{1-\eta_L V_{EG}} + \frac{5}{8} \frac{1+2\eta_T V_{EG}}{1-\eta_T V_{EG}} \right] E_{PP} \quad (1)$$

$$\eta_L = \frac{(E_{EG}/E_{PP})-1}{(E_{EG}/E_{PP})+\frac{2}{3}(d_{EG}/t_{EG})}$$

$$\eta_T = \frac{(E_{EG}/E_{PP})-1}{(E_{EG}/E_{PP})+2}$$

$$V_{EG} = \left[1+\left(\frac{\rho_{EG}}{\rho_{PP}}\right)\left(\frac{1-m_{EG}}{m_{EG}}\right) \right]^{-1}$$

where E_{EG} and E_{PP} are graphene modulus (1060 GPa) [16] and PP modulus (0.46 GPa), respectively. t_{EG} and d_{EG} are thickness (~1.75 nm) and diameter (~10 μm) of graphene platelets, respectively, which were prepared *via* the oxidation/exfoliation process [24]. V_{EG}, the volume fraction of

Table 2. Tensile mechanical properties of the neat PP and PP/EG nanocomposite films

Sample code	EG (wt%)	Yielding strength (MPa)	Yielding strain (%)	Breaking strength (MPa)	Breaking strain (%)	Initial modulus (MPa)
Neat PP	0.0	16.3±1.3	7.6±0.6	20.2±1.5	998.5±91.5	449.1±42.1
PP/EG	0.1	18.0±2.0	6.6±0.9	14.1±2.7	88.8±18.7	626.2±24.7
	0.3	19.3±4.6	5.1±1.6	14.7±4.1	23.4±9.9	741.4±90.9
	0.5	19.3±3.5	5.4±1.1	15.7±1.9	29.6±6.8	710.8±84.9
	0.7	19.4±3.8	4.7±1.1	16.1±3.7	23.2±6.5	731.9±83.8
	1.0	19.7±2.5	4.3±0.3	16.3±0.7	14.1±5.0	668.3±56.7
	3.0	22.8±6.0	4.6±0.9	16.7±3.3	7.6±1.9	733.6±116.5
	5.0	28.7±3.5	5.4±0.4	20.9±0.8	7.1±0.9	820.5±127.6
	7.0	28.1±2.7	4.9±0.3	28.1±2.7	4.9±0.3	841.0±216.5
	10.0	29.0±2.1	5.3±0.4	29.0±2.2	5.3±0.4	956.1±46.8

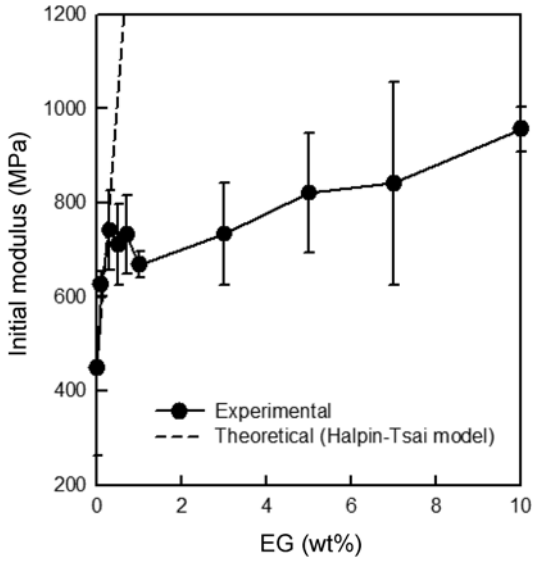

Figure 8. Initial modulus of the neat PP and its nanocomposite films as a function of EG content. The dashed line indicates the theoretical modulus predicted by the Halpin-Tsai model.

EG in the nanocomposites, which can be converted from the weight fraction of EG (m_{EG}), by adopting the graphite density (ρ_{EG}=1.9 g/cm^3) and the density (ρ_{PP}=0.9 g/cm^3) of PP with ~40 % crystallinity. As a result, the theoretical modulus calculated by the Halpin-Tsai equation was presented as a dotted line in Figure 8. The experimental initial moduli at 25 °C were quite consistent with the theoretical values for the nanocomposites with low EG contents below 0.5 wt%, but they were far lower than the theoretical values for the nanocomposites with high EG contents above 1.0 wt%. It must be mentioned that the moduli predicted by the Halpin-Tsai equation is based on the assumptions of the perfect interfacial adhesion between graphene platelets and PP matrix, the perfect 2-dimensional planar structure of graphene platelets of EG, and uniform dispersion of graphene platelets in the PP matrix. Therefore, it is speculated that the large difference between experimental and theoretical moduli for the nanocomposites with high EG contents above 1.0 wt% is owing to the partial aggregation of graphene platelets of EG in the PP matrix as well as the structural distortion and imperfection of graphene platelets. The presence of partial aggregates of disordered graphene platelets in the nanocomposites containing high EG contents above 3.0 wt% was evidenced by SEM images in Figure 3, as discussed above.

Conclusion

In this study, EG, which is composed of disordered graphene platelets and has high aspect ratio, was prepared via the oxidation/exfoliation process and it was adopted as the reinforcing nanofiller for PP matrix. PP-based nanocomposite films reinforced with 0.1~10.0 wt% EG were manufactured by efficient melt-mixing and compression. X-ray diffraction results demonstrated that, for all nanocomposite films, graphene platelets of EG remained in a disordered state in the PP matrix without influencing crystalline α-phase of PP. SEM images confirmed that the graphene platelets in the nanocomposites with EG contents less than 1.0 wt% were well dispersed in the PP matrix, while they were partially aggregated in the nanocomposites with EG contents more than 3.0 wt%. DSC cooling curves exhibited that the melt-crystallization temperatures of PP/EG nanocomposites increased slightly with the increment of EG content, indicating that graphene platelets of EG accelerated overall-crystallization of the PP matrix. Thermo-oxidative stability of PP/EG nanocomposites was highly improved by the presence of graphene platelets of EG. For instance, $T_{50\%}$ of the nanocomposite with 10.0 wt% EG under oxygen condition was enhanced by ~40 °C, compared with the neat PP. Electrical resistivities of the neat PP and its nanocomposite films were varied appreciably from ~10^{16} to ~10^6 Ω·cm with the EG content, especially at a certain EG

content between 1.0 and 3.0 wt%. Tensile mechanical results showed that breaking strength and initial modulus of the nanocomposite films were highly increased by the introduction of graphene platelets, while breaking strain were decreased. Initial moduli of PP/EG nanocomposite films increased steeply with increasing EG content up to ~0.5 wt% and then increased slightly at higher EG content. It was found that initial modulus (~956 MPa) of the nanocomposite film with 10.0 wt% EG was improved by 113 %, compared to the neat PP (~449 MPa).

Acknowledgement

This research was supported by Basic Science Program through the National Research Foundation of Korea (NRF) funded by the Ministry of Education, Science and Technology (2010-0011176).

References

1. N. Pasquini, Ed. "Polypropylene Handbook", 2nd ed, Hanser Gardner Publications, Cincinnati, Ohio, 2005.
2. E. Manias, *Nature Mater.*, **6**, 9 (2007).
3. D. W. Schaefer and R. S. Justice, *Macromolecules*, **40**, 8501 (2007).
4. E. S. Trofimchuk, E. A. Nesterova, I. B. Meshkov, N. I. Nikonorova, A. M. Muzafarov, and N. P. Bakeev, *Macromolecules*, **40**, 9111 (2007).
5. S. Barus, M. Zanetti, M. Lazzari, and L. Costa, *Polymer*, **50**, 2595 (2009).
6. J. H. Lee and Y. G. Jeong, *J. Appl. Polym. Sci.*, **115**, 1039 (2010).
7. E. P. Giannelis, *Adv. Mater.*, **8**, 29 (1996).
8. A. Okada and A. Usuki, *Macromol. Mater. Eng.*, **291**, 1449 (2006).
9. D. R. Paul and L. M. Robeson, *Polymer*, **49**, 3187 (2008).
10. X.-L. Xie, Y.-W. Mai, and X.-P. Zhou, *Mater. Sci. Eng. R*, **49**, 89 (2005).
11. M. Moniruzzaman and K. I. Winey, *Macromolecules*, **39**, 5194 (2006).
12. C. McClory, S. J. Chin, and T. McNally, *Aust. J. Chem.*, **62**, 762 (2009).
13. M. H. Jee, J. S. Lee, J. Y. Lee, Y. G. Jeong, and D. H. Baik, *Fiber. Polym.*, **11**, 1 (2010).
14. K. S. Novoselov, A. K. Geim, S. V. Morozov, D. Jiang, Y. Zhang, S. V. Dubonos, I. V. Grigorieva, and A. A. Firsov, *Science*, **306**, 666 (2004).
15. Y. Zhang, Y.-W. Tan, H. L. Stomer, and P. Kim, *Nature*, **438**, 201 (2005).
16. C. Lee, X. Wei, J. W. Kysar, and J. Hone, *Science*, **321**, 385 (2008).
17. J.-W. Shen, X.-M. Chen, and W.-Y. Huang, *J. Appl. Polym. Sci.*, **88**, 1864 (2003).
18. V. Causin, C. Marega, A. Marigo, G. Ferrara, and A. Ferraro, *Eur. Polym. J.*, **42**, 3153 (2006).
19. K. Kalaitzidou, H. Fukushima, and L. T. Drzal, *Carbon*, **45**, 1446 (2007).
20. K. Kalaitzidou, H. Fukushima, and L. T. Drzal, *Compos. Sci. Technol.*, **67**, 2045 (2007).
21. K. Kalaitzidou, H. Fukushima, P. Askeland, and L. T. Drzal, *J. Mater. Sci.*, **43**, 2895 (2008).
22. K. Wakabayashi, C. Pierre, D. A. Dikin, R. S. Ruoff, T. Ramanathan, L. C. Brinson, and J. M. Torkelson, *Macromolecules*, **41**, 1905 (2008).
23. H. C. Schniepp, J.-L. Li, M. J. McAllister, H. Sai, M. Herrera-Alonso, D. H. Adamson, R. K. Prudhomme, R. Car, D. A. Saville, and I. A. Aksay, *J. Phys. Chem. B*, **110**, 8535 (2006).
24. M. J. McAllister, J.-L. Li, D. H. Adamson, H. C. Schniepp, A. A. Abdala, J. Liu, M. Herrera-Alonso, D. L. Milius, R. Car, R. K. Prudhomme, and I. A. Aksay, *Chem. Mater.*, **19**, 4396 (2007).
25. L. Staudenmaier, *Ber. Dtsch. Bot. Ges.*, **31**, 1481 (1898).
26. X. Zhao, Q. Zhang, D. Chen, and P. Lu, *Macromolecules*, **43**, 2357 (2010).
27. J. C. Halpin and S. W. Tsai, "Effects of Environmental Factors on Composite Materials", US Air Force Materials Laboratory, Dayton, Ohio, 1969.
28. J. C. Halpin and J. L. Kardos, *Polym. Eng. Sci.*, **16**, 344 (1976).
29. P. K. Mallick, "Fiber-reinforced Composites: Material Manufacturing and Design", Marcel Dekker Inc., New York, 1993.